

NeLF: Practical Novel View Synthesis with Neural Light Field

Celong Liu
OPPO US Research Center
InnoPeak Technology Inc.
Palo Alto, California, USA
celong.liu@oppo.com

Zhong Li
OPPO US Research Center
InnoPeak Technology Inc.
Palo Alto, California, USA
zhong.li@oppo.com

Junsong Yuan
University at Buffalo
State University of New York.
Buffalo, New York, USA
jsyuan@buffalo.edu

Yi Xu
OPPO US Research Center
InnoPeak Technology Inc.
Palo Alto, California, USA
yi.xu@oppo.com

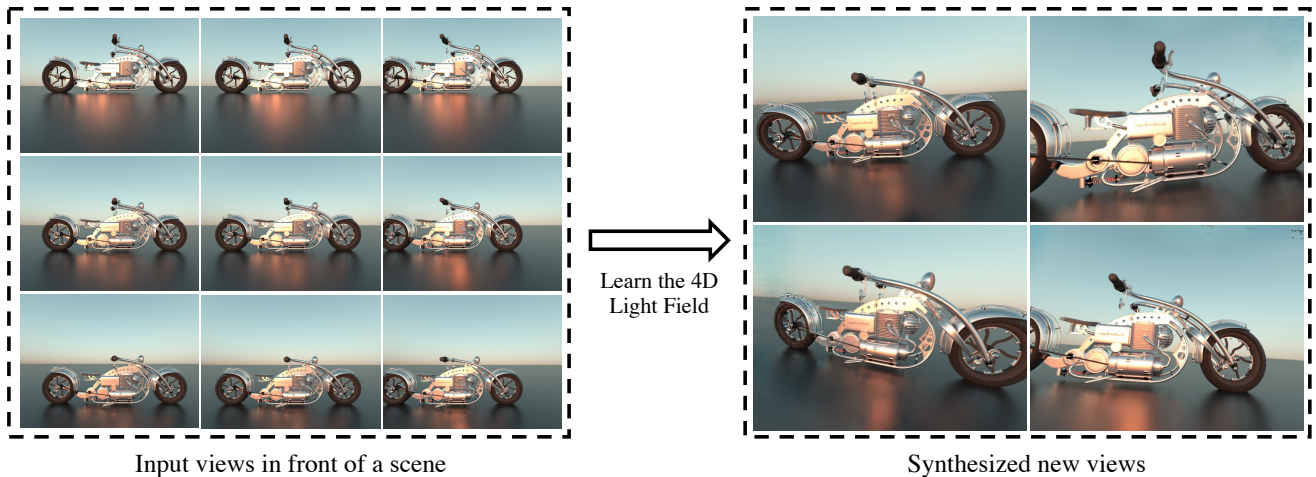


Figure 1: Given a set of images captured in front of a scene, **Neural 4D Light Field (NeLF)** uses an implicit neural representation to learn the mapping from rays to color values. With the learned model, novel views can be synthesized by predicting the color of each ray.

Abstract

In this paper, we present an efficient and robust deep learning solution for novel view synthesis of complex scenes. In our approach, a 3D scene is represented as a light field, i.e., a set of rays, each of which has a corresponding color when reaching the image plane. For efficient novel view rendering, we adopt a 4D parameterization of the light field, where each ray is characterized by a 4D parameter. We then formulate the light field as a 4D function that maps

4D coordinates to corresponding color values. We train a deep fully connected network to optimize this implicit function and memorize the 3D scene. Then, the scene-specific model is used to synthesize novel views. Different from previous light field approaches which require dense view sampling to reliably render novel views, our method can render novel views by sampling rays and querying the color for each ray from the network directly, thus enabling high-quality light field rendering with a sparser set of training images. Our method achieves state-of-the-art novel view syn-

thesis results while maintaining an interactive frame rate.

1 Introduction

Novel view synthesis has long been studied by the computer vision and computer graphics community. It has many applications in multimedia, AR/VR, gaming, etc. Traditional computer vision approaches such as multi-view stereo (MVS) and structure-from-motion (SfM) aim to build a geometric representation of the scene first. An alternative approach is image-based rendering [14, 7, 3], where no underlying geometric model or only a simple proxy is needed. These methods can achieve photo-realistic rendering. However, a typical light field setup prefers a dense sampling of views around a scene. It thus limits practical use of such an approach.

With the recent advancement of neural rendering [36], photo-realistic rendering with only a sparse set of inputs can be achieved. One approach is to use an explicit geometric representation of a scene reconstructed using a traditional computer vision pipeline and learning-based rendering. Object-specific or category-specific meshes or multi-plane images (MPI) [45] can be used as the representation. However, these explicit representations do not allow a network to learn the optimal representation of the scene. To achieve this, volume-based representations can be used [17]. However, they typically require a large amount of memory space, especially for complex scenes.

Memory-efficient implicit representations have gained interests from the research community. For example, surface-based implicit representations can achieve state-of-the-art results and can provide a high-quality reconstruction of the scene geometry [12]. However, surface-based representations face challenges when dealing with complex lighting and geometry, such as transparency, translucency, and thin geometric structures. More recently, volume-based implicit representation achieves remarkable rendering results (e.g., NeRF [22]) and inspires follow-up research. One drawback of NeRF, nevertheless, is the time complexity of rendering, which prohibits real-time applications. Although there have been many efforts to accelerate NeRF, they typically require ground-truth depth to train or rely on additional storage to achieve faster rendering.

We propose an efficient novel view synthesis framework, which we call Neural 4D Light Field (NeLF). We define a scene as an implicit function that maps 4D light field rays to corresponding color values. This function can be implemented as a Multilayer Perceptron (MLP) and can be learned using only a sparse set of calibrated images placed around the scene. This formulation allows the color of a camera ray to be learned directly by the network and does

not require a time-consuming ray-marcher during rendering. Thus, NeLF achieves 1000x speedup over NeRF during inference, while producing similar or even better rendering quality. Unlike NeRF, NeLF does not optimize for the scene geometry explicitly. Thus, a 3D surface or a depth map cannot be directly produced by our proposed NeLF. Moreover, our light field setup limits the novel viewpoints to be on the same side of the cameras, e.g. front views only. Despite these constraints, we argue that for many applications such as teleconferencing, these are reasonable trade-offs to gain much faster inference speed with high quality rendering. To enable high-quality novel view rendering, we propose a novel Fourier Sparsity Loss, which regularizes the similarity in the frequency domain between input images and synthesized images. Moreover, we propose a Ray Bundle Loss that solves the aliasing problem caused by the discretization of pixels from the input data. These two treatments allow us to train NeLF to synthesize high-quality novel views from a sparse set of input images. We show state-of-the-art novel view synthesis results on benchmark datasets. The comparisons with existing approaches also validate the efficiency and effectiveness of our proposed method.

2 Related Work

Our work builds upon previous work in traditional image-based rendering and implicit-function-based neural scene representation. In the following sections, we will review these fields and beyond in detail.

2.1 Image-based Rendering

For novel view synthesis, image-based rendering has been studied as an alternative to geometric methods such as multi-view stereo or structure from motion. In the seminal work of light field rendering [14], a 5D radiance field is reduced to a 4D light field considering the radiance along a ray remains constant in free space. The ray set in a light field can be parameterized in different ways, among which two-plane parameterization is the most common one. Rendering novel views from the light field involves extracting corresponding 2D slices from the 4D light field. To achieve better view interpolation, approximate geometry can be used [7, 3]. Visual effects of variable focus and variable depth-of-field can also be achieved using light field [10].

With the advancement of deep learning, a few learning-based methods have been proposed to improve the traditional light field. For example, LFGAN [4] can learn texture and geometry information from light field data sets and in turn predict a small light field from one RGB image. [20] enables high-quality reconstruction of a light field by learning the geometric features hierarchically using a residual

network. [40] integrates an anti-aliasing module in a network to reduce the artifacts in the reconstructed light field. Our method learns an implicit function of the light field and achieves high-quality reconstruction with very sparse input while handling aliasing problem.

2.2 Neural Scene Representation

Neural rendering is an emerging field. One of the most important applications of neural rendering is novel view synthesis. A comprehensive survey of the topic can be found in [36].

An explicit geometric model can be used as the representation of a scene. [26] creates a proxy geometry of the scene using structure from motion and multi-view stereo (MVS). Then, a recurrent encoder-decoder network is used to synthesize new views from nearby views. To improve blending on imperfect meshes from MVS, [9] uses predicted weights from a network to perform blending. A high-quality parameterized mesh of the human body [44] and category-specific mesh reconstruction [11] can also be used as the proxy. Recently, Multi-plane Image (MPI) [45] has gained popularity. [45] learns to predict MPIs from stereo images. The range of novel views is later improved by [34]. [5] uses learned gradient descent to generate an MPI from a set of sparse inputs. [21] uses an MPI representation for turning each sampled view into a local light field. NeX [39] represents each pixel of an MPI with a linear combination of basis functions and achieves state-of-the-art rendering results in real-time. MPI representation might typically lead to stack-of-cards artifacts. Moreover, these representations do not allow the network to learn the optimal representation of a scene. Volume-based representation provides such capability for scene-specific scenarios. [31] trains a network to reconstruct both the geometry and appearance of a scene on a 3D grid. For dynamic scenes, Neural Volumes (NV) [17] uses an encoder-decoder network to convert input images into a 3D volume representation. [18] extends NV using a mixture of volumetric primitives to achieve better and faster rendering. While volume-based representations allow for learning the 3D structure, they require large memory space, especially for large scenes.

Implicit-function-based approaches provide memory-efficient alternatives to explicit representations, while still allowing learning the 3D structure of the scene. Implicit representations can be categorized as implicit surface-based and implicit volume-based approaches. PIFU [27] uses implicit functions to represent both surface geometry and texture. SRN [32] maps 3D coordinates to a local feature embedding at these coordinates. Then, a trained ray-marcher and a pixel generator are used to render novel views. IDR [41] uses an implicit Signed Distance Function (SDF) to model an object and achieves state-of-the-art re-

sults on 3D surface reconstruction while learning geometry, appearance, and camera all at once. Neural Lumigraph [12] provides even better rendering quality by utilizing a sinusoidal representation network (SIREN) to model the SDF.

Our work is inspired by NeRF [22], which uses a network to map continuous 5D coordinates (location and view direction) to volume density and view-dependent radiance. It achieves remarkable novel view synthesis results. Recent works have extended NeRF to support novel illumination conditions [33], rendering from unstructured image collections from the internet [19], large-scale unbounded scenes [43], unknown camera parameters [37], anti-aliasing [1], deformable models [24], etc. A lot of effort has been put into speeding up rendering with NeRF. DOnNeRF [23] places samples around scene surfaces by predicting sample locations along each ray. However, transparent objects will pose issues and it requires ground-truth depth for training. FastNeRF [6] achieves 200fps by factoring NeRF into a position-dependent network and a view-dependent network. This allows efficient caching of network outputs during rendering. [42] trains a NeRF-SH network, which maps coordinates to spherical harmonic coefficients and pre-samples the NeRF-SH into a sparse voxel-based octree structure. These pre-sampling approaches sacrifice additional memory storage for speedups. NSVF [16] represents a scene using a set of NeRF-like implicit fields defined on voxels and uses a sparse octree to achieve 10x speedup over NeRF during rendering. However, the performance is scene-dependent. KiloNeRF [25] decomposes a scene into a grid of voxels and uses a smaller NeRF for each voxel. Storage costs will increase when more networks are used. Using AutoInt [15], calculations of any definite integral can be done in two network evaluations; this achieves 10x acceleration, but rendering quality is decreased. Compared with these approaches, our method achieves 1000x speedup over NeRF by representing the scene with an implicit 4D light field without any additional pre-sampling or storage overhead.

3 Our Method

In Figure 2, we illustrate the pipeline of our system. In the following sections, we will first briefly discuss the light field, followed by our NeLF representation and the proposed loss functions. We will also discuss our training strategies.

3.1 4D Light Field Representation

All possible light rays in a space can be described by a 5D plenoptic function. Since radiance along a ray is constant if viewed from outside of the convex hull of the scene, this 5D function can be reduced to a 4D light field [14, 7].

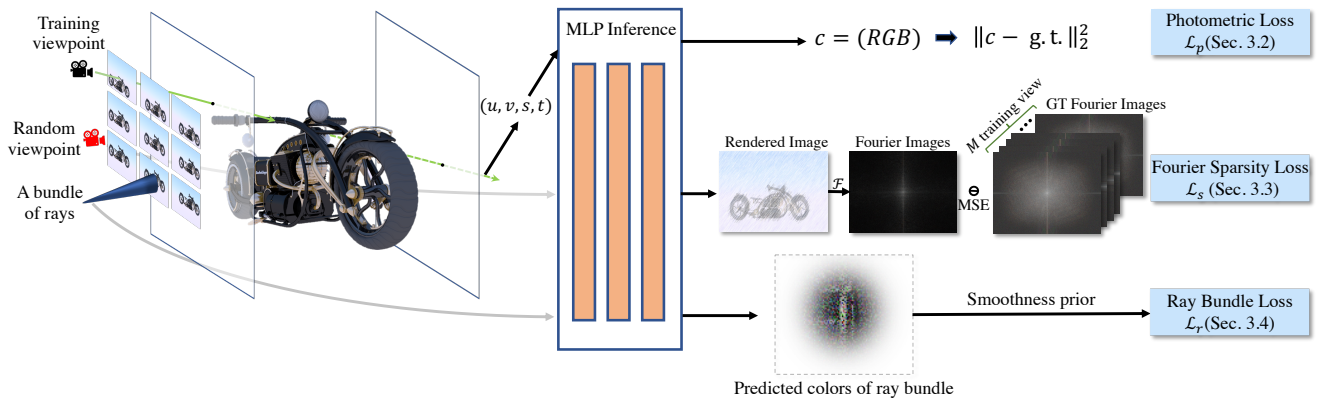


Figure 2: An overview of the Neural 4D Light Field (NeLF). For a set of sampled rays from training images, their 4D coordinates and the corresponding color values can be obtained. The input for NeLF is the 4D coordinate of a ray (query) and the output is its RGB color. By optimizing the difference between the predicted colors and ground-truth colors, NeLF can faithfully learn the mapping between a 4D coordinate that characterizes the ray and its color. We also enforce the frequency distribution similarity (the Fourier Sparsity Loss \mathcal{L}_s , see Sec. 3.3) and neighboring ray smoothness (the Ray Bundle Loss \mathcal{L}_r , see Sec. 3.4) to avoid overfitting and to solve aliasing problems, respectively.

The most common parameterization is a two-plane model shown in Fig. 3. Each ray from the camera to the scene will intersect with the two planes. Thus, we can represent each ray using the coordinates of the intersections, (u, v) and (s, t) , or simply a 4D coordinate (u, v, s, t) . Using this representation, all rays from the object to one side of the two planes can be uniquely determined by a 4D coordinate.

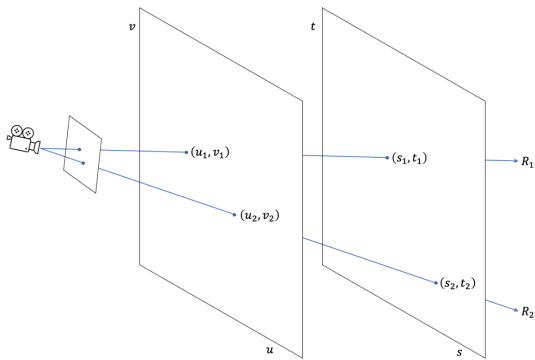


Figure 3: The 4D light field representation. Each ray is characterized by 4 parameters (u, v) and (s, t) , which uniquely locates the ray.

Based on this representation, rendering a novel view can be done by querying all the rays from the center of projection to every pixel on the camera’s image plane. We denote them as $\{R_1, R_2, \dots, R_N\}$, where N is the total number of pixels. Then, for the i -th ray R_i , we can obtain its 4D coordinate (u_i, v_i, s_i, t_i) by computing its intersections with the two planes. If a function f maps the continuous 4D co-

ordinates to color values, we can obtain the color of R_i by evaluating the function $f(u_i, v_i, s_i, t_i)$. In the next section, we will introduce Neural 4D Light Field (NeLF) for reconstructing this mapping function f .

3.2 Neural 4D Light Field Reconstruction

We formulate the mapping function f as a Multilayer Perceptron (MLP). The input of this MLP is a 4D coordinate and the output is RGB color. Hence, we have

$$(u, v, s, t) \rightarrow \begin{matrix} \text{MLP} \\ \text{with } \Theta \end{matrix} \rightarrow (R, G, B), \quad (1)$$

where Θ represents the trainable parameters. The goal of the network is to learn the mapping function from training data.

Training Data: for a given scene, the training data comes from a set of captured images $\{I_1, I_2, \dots, I_M\}$, where M is the total number of images. Assuming the camera pose for each image is known or obtainable, for each image $I_k (k = 1, \dots, M)$, we can traverse its pixels and generate all corresponding rays $\{R_1^k, R_2^k, \dots, R_{N_k}^k\}$, where N_k is the total number of pixels in the k -th image. Based on the 4D light field representation, all 4D coordinates $\{(u_1^k, v_1^k, s_1^k, t_1^k), \dots, (u_{N_k}^k, v_{N_k}^k, s_{N_k}^k, t_{N_k}^k)\}$, $(k = 1, \dots, M)$, can be obtained. On the other hand, the color for

each pixel is known from the input images. To this end, we have constructed a collection of sample mappings from 4D coordinates to color values $(u_i^k, v_i^k, s_i^k, t_i^k) \rightarrow c_i^k$, ($k = 1 \dots M, i = 1 \dots N_k$), where c_i^k is the color of the i -th pixel on the k -th image. By feeding this training data to the MLP network, the parameters Θ can be learned by minimizing the following photometric loss \mathcal{L}_p :

$$\mathcal{L}_p = \sum_{k=1}^M \sum_{i=1}^{N_k} \|f(u_i^k, v_i^k, s_i^k, t_i^k | \Theta) - c_i^k\|_2 \quad (2)$$

A vanilla MLP is not able to encode the high frequency information of a scene. Recent works show that using a high dimension embedding [35], or using periodic activation functions [30] can help recover fine details. In this work, we adopt the position embedding following [35]. We first pass the 4D coordinates to the embedder and then feed the embedded vectors into the network. Specifically, for a 4D coordinate $\mathbf{v} = (u_i^k, v_i^k, s_i^k, t_i^k)^T$, the embedder will map it to:

$$\gamma(\mathbf{v}) = [\cos(2\pi\mathbf{b}_1^T \mathbf{v}), \sin(2\pi\mathbf{b}_1^T \mathbf{v}), \dots, \cos(2\pi\mathbf{b}_L^T \mathbf{v}), \sin(2\pi\mathbf{b}_L^T \mathbf{v})], \quad (3)$$

where each element in $\mathbf{B} = [\mathbf{b}_1^T, \mathbf{b}_2^T, \dots, \mathbf{b}_L^T] \in \mathbb{R}^{L \times 4}$ is sampled from $\mathcal{N}(0, \sigma^2)$, where σ and L are chosen for each scene with a hyper-parameter grid searching. In our experiments, we found $\sigma = 16$ and $L = 256$ work best for most of the scenes we tested. Note that using periodic activation functions such as the SIREN [30] can potentially work as well.

In Fig. 4, we demonstrate an example of capturing images to train our neural 4D light field representation with a camera array. In this example, the cameras are placed on a plane parallel to the parameterization light slabs, and the image plane for each camera is parallel to the light slabs as well. This configuration simplifies the ray parameterization; however, our pipeline has no restriction on the camera positioning strategy; the cameras can be placed in a slightly unstructured pattern in front of the scene. In Sec. XX, we show novel view synthesis results using such a camera configuration.

Rendering: Given a viewpoint \mathcal{V} , we can render a novel view $\mathcal{R}(\mathcal{V})$ by evaluating the learned mapping function f . With the camera pose and the desired rendering resolution $\{W^\mathcal{V}, H^\mathcal{V}\}$, we sample all rays $\{R_1^\mathcal{V}, R_2^\mathcal{V}, \dots, R_{N_\mathcal{V}}^\mathcal{V}\}$, where $N_\mathcal{V} = W^\mathcal{V} \times H^\mathcal{V}$ is the number of pixels to be rendered. We can further calculate the 4D coordinates $\{(u_i^\mathcal{V}, v_i^\mathcal{V}, s_i^\mathcal{V}, t_i^\mathcal{V})\}$ for each ray $R_i^\mathcal{V}$, ($i = 1 \dots N_\mathcal{V}$). We then formulate the rendering process \mathcal{R} as $N_\mathcal{V}$ evaluations of the mapping function f :

$$\mathcal{R}(\mathcal{V}) = \{f(u_i^\mathcal{V}, v_i^\mathcal{V}, s_i^\mathcal{V}, t_i^\mathcal{V} | \Theta), i = 1, \dots, N_\mathcal{V}\}. \quad (4)$$

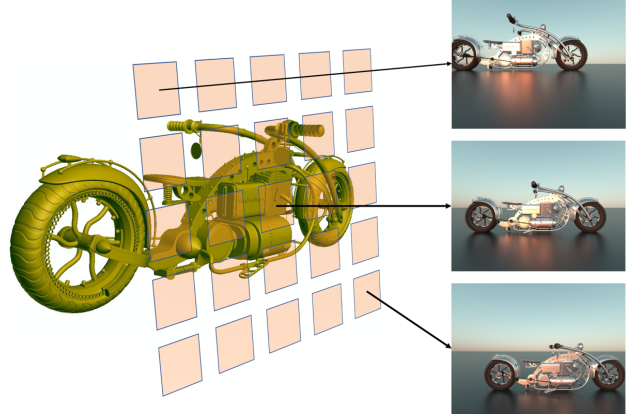


Figure 4: Image capturing with camera array.

Comparison with NeRF: Although our work is inspired by NeRF [22], there are some key distinctions. NeRF represents the continuous scene function as a 5D radiance field. Such a representation has redundancy, i.e., color along a ray is constant in free space. By restricting the novel viewpoints to be outside of the convex hull of the object, the 5D radiance field can be reduced to a light field in a lower dimension. Moreover, because NeLF learns the color of the rays directly, rendering becomes significantly faster without requiring a time-consuming ray marching process like NeRF. The disadvantage of NeLF is that it does not have the capability of learning the 3D scene geometry like NeRF. We argue that for certain applications, this is a small price to pay. In Table 1, we summarize the differences between NeLF and NeRF.

Table 1: The comparisons between our proposed NeLF and NeRF [22].

	NeRF	NeLF
Input	5D	4D
Output	radiance, density	color
Viewpoint range	360°	front views
Rendering method	raymarching	direct evaluation
Rendering speed	slow	fast
Memory consumption	small	small
Explicit geometry	yes	no
High-quality rendering	yes	yes

3.3 Fourier Sparsity

Learning the MLP solely by optimizing \mathcal{L}_p will let the network quickly overfit the data and remember the relationships between the 4D coordinates and colors existing in the training data. As a result, the MLP will overfit the input viewpoints and cannot give reasonable *novel* view synthesis

results. In the first row of Figure 5, we show the results of synthesizing novel views by using an overfitted MLP. The leftmost and rightmost views are reconstructed images from two viewpoints in the training data. The middle view is an in-between *novel* view not present in the training set. Its rendering quality is dramatically degraded. The network simply remembers the colors for all the rays in the training set without learning the representation of the scene. Therefore, it will predict unreliable results for unseen rays. In the second row of Figure 5, we show the corresponding ground-truth images for comparison.

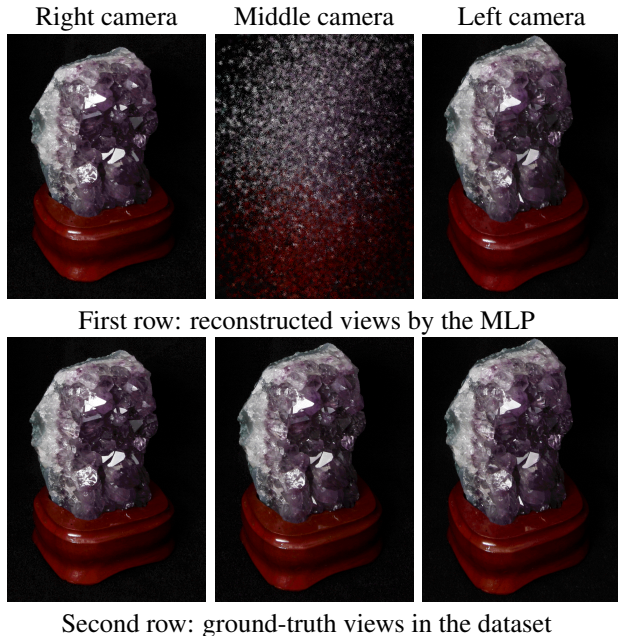


Figure 5: View synthesis results by overfitted network. The images in the first row are rendered by the MLP. The images in the second row are the ground truth. The leftmost and rightmost images are two consequent views from training data, and they can be reconstructed faithfully by the MLP. The middle view is a novel view not in the training set, and the MLP fails to render the correct result.

Inspired by the sparsity nature of light fields in the frequency domain [28], we propose a Fourier Sparsity Loss to regularize the learning. For a given scene, we assume that nearby views have similar frequency distribution in the frequency domain. If the network synthesizes a novel view successfully, the rendered image will have a similar frequency distribution as the input data. As an example, in Figure 6, we visualize the frequency distribution of the three views from Figure 5.

We propose an approach to encourage rendered novel views to have a similar frequency distribution as the images in the training set. For each training image $I_k (k = 1, \dots, M)$, we compute its frequency distribution $\mathcal{F}(I_k)$ by

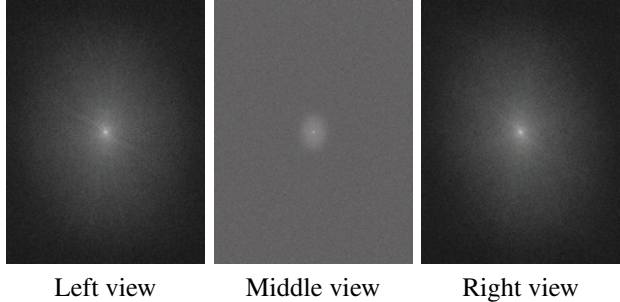


Figure 6: Fourier transform results for the three images from Figure 5 top row. The correct views (leftmost view and rightmost view) have similar frequency distribution, while the failed view (middle view) has a different distribution.

applying the Fourier transform $\mathcal{F}(\cdot)$. Based on the camera pose for each training image, we sample a set of random novel viewpoints $\{\mathcal{V}_1, \mathcal{V}_2, \dots, \mathcal{V}_J\}$, where J is the number of novel viewpoints (see 4.1 Training Strategies for detail). For simplification, we compare the frequency distribution of a novel viewpoint with all training images, since the dataset we used has small baselines. However, it is trivial to generalize to large baseline settings by only enforcing similarity with neighboring views. Therefore, we define the Fourier Sparsity Loss \mathcal{L}_s as follows:

$$\mathcal{L}_s = \sum_{k=1}^J \sum_{i=1}^M \|\mathcal{F}(\mathcal{R}(\mathcal{V}_k)) - \mathcal{F}(I_M)\|_2 \quad (5)$$

Training with \mathcal{L}_s will encourage the MLP to learn the optimal representation of the scene. Specifically, in addition to remembering the color of a set of rays, the MLP will learn the information of color changes, i.e., the first-order gradient of colors, in 4D space.

3.4 Ray Bundle Loss

Aliasing is a common issue in light field rendering [40]. In our work, although NeLF models the rays in continuous 4D space, the training rays are sampled on discrete pixels due to the imaging process. With the photometric loss \mathcal{L}_p and Fourier Sparsity Loss \mathcal{L}_s , the network will be encouraged to remember the color for each ray and recover the frequency distribution. However, there is no guarantee that the predicted colors for rays in-between neighboring rays are smooth and this leads to aliasing. Inspired by the conical frustum introduced in [1] to solve this problem for NeRF, we propose a Ray Bundle Loss \mathcal{L}_r based on the following heuristics: for a ray R cast from a viewpoint, we cast T rays $\{R_1, R_2, \dots, R_T\}$ from the same origin but with slightly different directions. The rays with smaller angles to R are more likely to have the same color as R . Therefore, we de-

Table 2: Average scores across 264 views for each scene in the Stanford Light Field dataset.

	PSNR \uparrow					SSIM \uparrow				
	NeRF	LLFF	SRN	NSVF	NeLF (Ours)	NeRF	LLFF	SRN	NSVF	NeLF (Ours)
Amethyst	38.014	36.057	34.497	36.422	39.208	0.941	0.886	0.819	0.894	0.952
Bracelet	34.656	33.252	32.356	33.551	35.750	0.934	0.853	0.735	0.867	0.938
Tarot Cards (large)	32.361	31.025	30.274	31.396	33.872	0.874	0.718	0.568	0.746	0.887
Tarot Cards (small)	33.015	31.607	30.190	31.952	34.055	0.883	0.763	0.573	0.784	0.889
Chess	38.496	36.377	34.157	36.985	39.109	0.953	0.918	0.841	0.925	0.949
Eucalyptus Flowers	38.387	36.905	35.812	37.219	40.189	0.937	0.887	0.842	0.894	0.954
Jelly Beans	43.151	41.350	38.977	41.819	43.335	0.985	0.976	0.957	0.978	0.983
Lego Knights	37.057	35.033	33.096	35.693	38.470	0.936	0.885	0.801	0.896	0.939
Lego Truck	38.358	36.393	34.795	36.815	39.483	0.939	0.890	0.820	0.898	0.943
Lego Bulldozer	37.156	35.183	33.723	35.618	37.799	0.931	0.872	0.789	0.882	0.929
The Stanford Bunny	40.797	38.122	35.335	38.671	41.178	0.964	0.935	0.887	0.941	0.966
Treasure Chest	36.424	34.857	33.469	35.211	37.725	0.925	0.853	0.764	0.862	0.941

fine \mathcal{L}_r as a weighted sum of l_2 terms over surrounding rays as follows:

$$\mathcal{L}_r = \sum_{i=1}^T e^{-\frac{\langle R, R_i \rangle}{\theta}} \|f(u, v, s, t | \Theta) - f(u_i, v_i, s_i, t_i | \Theta)\|_2, \quad (6)$$

where $\{u, v, s, t\}$ and $\{u_i, v_i, s_i, t_i\}$ are the 4D coordinates for ray R and R_i ($i = 1, 2, \dots, T$) respectively; $\langle R, R_i \rangle$ denotes the angle between R and R_i ; and θ is the weighting parameter. We discuss the effect of using different values for θ in Sec. 4.3. In our experiments, we found $\theta = 1.5^\circ$ works best for most of the scenes we tested. This value is correlated to the size of a pixel in the imaging setting.

4 Experimental Results

We first discuss the implementation details of NeLF. Then we perform quantitative and qualitative evaluations against state-of-the-art methods for novel view synthesis. We also provide studies to analyze the effectiveness of the Fourier Sparsity Loss \mathcal{L}_s and the Ray Bundle Loss \mathcal{L}_r .

4.1 Training Strategies

We train the MLP on the following overall loss function:

$$\mathcal{L} = \mathcal{L}_p + \lambda_s \mathcal{L}_s + \lambda_r \mathcal{L}_r, \quad (7)$$

where the weighting coefficients are $\lambda_s = 1.92$ and $\lambda_r = 0.074$. These parameters are fine-tuned by mixing the manual tuning and grid search tuning. This set of parameters works best for the scenes we tested. Grid search can be used to automatically find optimal parameters for a specific scene, but will lead to longer training time.

During training, we randomly select a batch of camera rays from the training set at each iteration. By passing them

to the MLP to predict the color of each ray, we calculate \mathcal{L}_p and back-propagate the error.

To calculate \mathcal{L}_s , in each iteration, we randomly generate a camera whose position is within the convex hull of all cameras of the training images. The viewing direction of the generated camera has a random offset from the z -direction, which is perpendicular to the two light slabs. The range of this offset is estimated by $\arctan(d/h)$, where d is the smallest distance from the selected camera to the convex hull of the training cameras, and h is the distance from the selected camera to the st -plane. This ensures the selected camera will look at the scene of interest.

To calculate \mathcal{L}_p , in each iteration, we sample a batch of camera rays from the training set randomly and generate another batch of rays using the same rules as the camera generation for \mathcal{L}_s . For each ray R in the two batches, we cast T rays from the origin of R , and the angle between R and each cast ray is sampled from $\mathcal{N}(0, \theta^2)$ where the negative angles will be skipped. We use $T = 16$ neighboring rays in all of our experiments.

The embedded input vector $\gamma(\mathbf{v})$ is passed through 6 fully-connected ReLU layers, each of which has 256 channels, and the final layer with a sigmoid activation to output the predicted color. For model training, we set the ray batch size in each iteration to 32768 for both \mathcal{L}_p and \mathcal{L}_r . We train the MLP for 200K iterations using the Adam optimizer [13]. The initial learning rate is 1×10^{-3} and is reduced by half every 20k iterations. To train the NeLF on a scene with 25 input images with a resolution of 1536×1280 , it will take 8 hours using 4 Nvidia V100 cards.

4.2 Comparison with State-of-the-Art Methods

In this section, we demonstrate the qualitative results of novel view synthesis and compare them with current top-performing approaches: NeRF [22], LLFF [21], SRN [32], and NSVF [16]. We evaluate the models on the Stanford

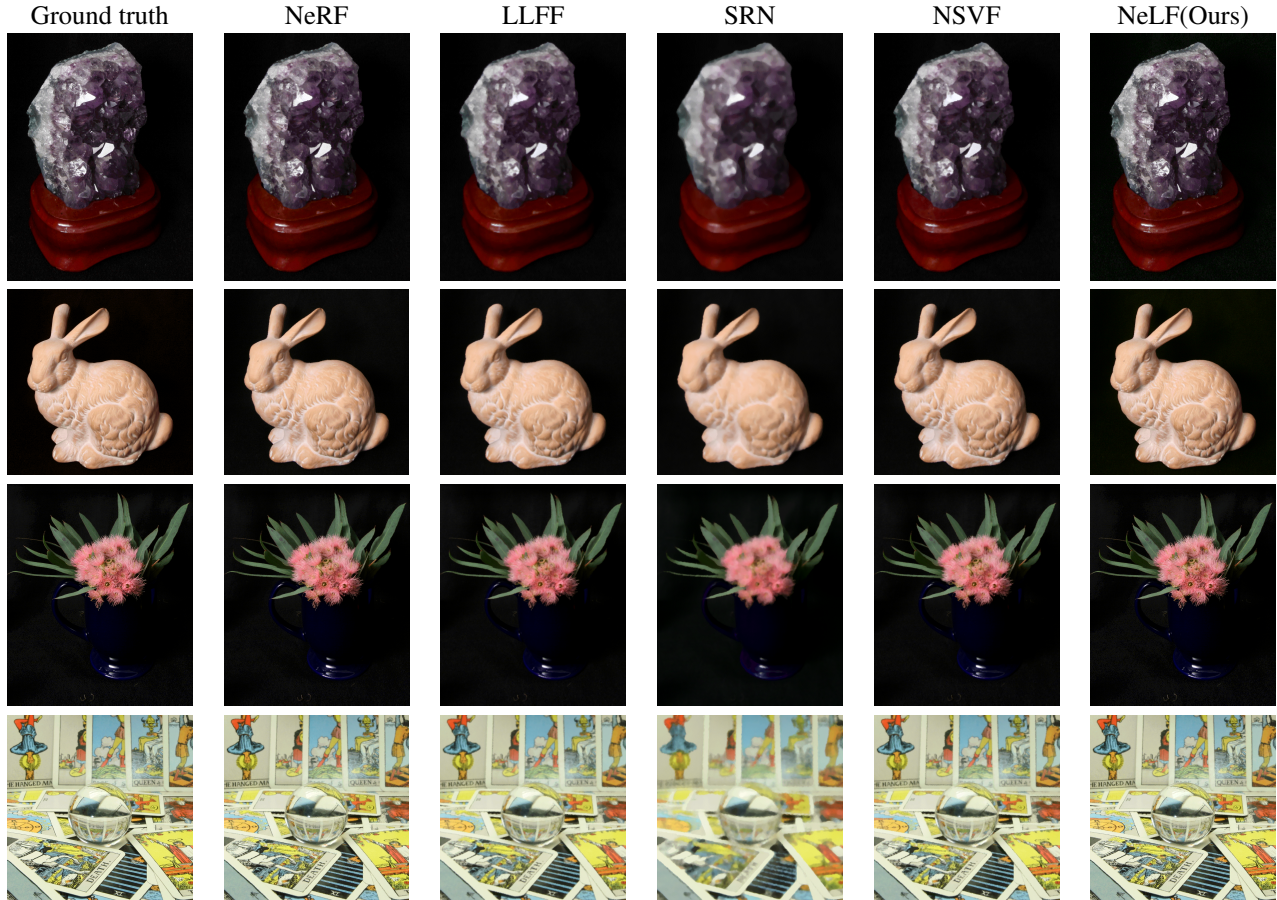


Figure 7: Qualitative results on test views from 4 scenes in the Stanford Light Field dataset. Our method captures more complete details than LLFF, SRN and NSVF in all scenes, and it is slightly better than NeRF when recovering high frequency features in scenes.

Light Field dataset [38]. In this dataset, each scene is captured by a 17×17 camera rig. For each scene, we use the 5×5 evenly sampled subset as the training data and use the remaining 264 views as the testing data. We use the same train/test split for all the models used in the experiments and evaluate results using two metrics: PSNR (Peak Signal-to-Noise Ratio, higher is better) and SSIM (Structural Similarity Index Measure, higher is better).

In Table 2, we report the scores for the Stanford Light Field dataset. For each scene, we calculate the scores by averaging across the 264 views in the test split. Our method produces the highest PSNR and has very close SSIM with NeRF. In Table 3, we report the storage usage for each model and the average per-frame inference time for each model. NeLF achieves a similar scene compression capability with a 1000x speedup compared with NeRF.

In Figure 7, qualitative comparisons are provided. The four scenes are *Amethyst*, *The Stanford Bunny*, *Eucalyptus*

Table 3: The storage usage for each model and average per-frame inference time for each method on the Stanford Light Field dataset.

	Model Size	Time / Frame
NeRF	9.1M	100s
LLFF	122M	650ms
SRN	630M	870ms
NSVF	16M	12s
NeLF (Ours)	8.1M	100ms

Flowers, and *Tarot Cards (small)* from the dataset. The rendering results by SRN are generally overly smooth. Novel views synthesized by LLFF and NSVF are better, but not as good as NeRF and NeLF. NeLF can achieve photo-realistic results that are close to or even slightly better than NeRF on various scenes with complex geometry (e.g. this structures) and lighting effects (e.g., reflections, refractions, etc.).

To further investigate the difference in terms of rendering

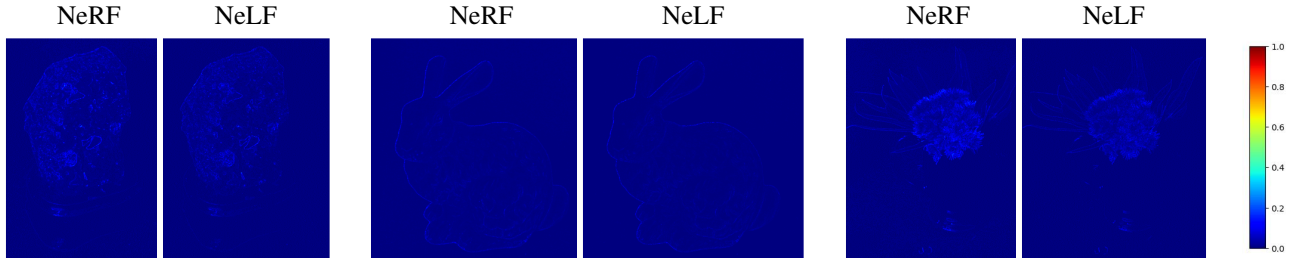


Figure 8: Color maps of the difference between the ground-truth view and the reconstructed view (using NeRF and NeLF) on three scenes from the Stanford Light Field dataset. In most flat regions, the difference is close to zero for both NeRF and NeLF. NeLF has a smaller reconstruction error on high-frequency areas than NeRF.

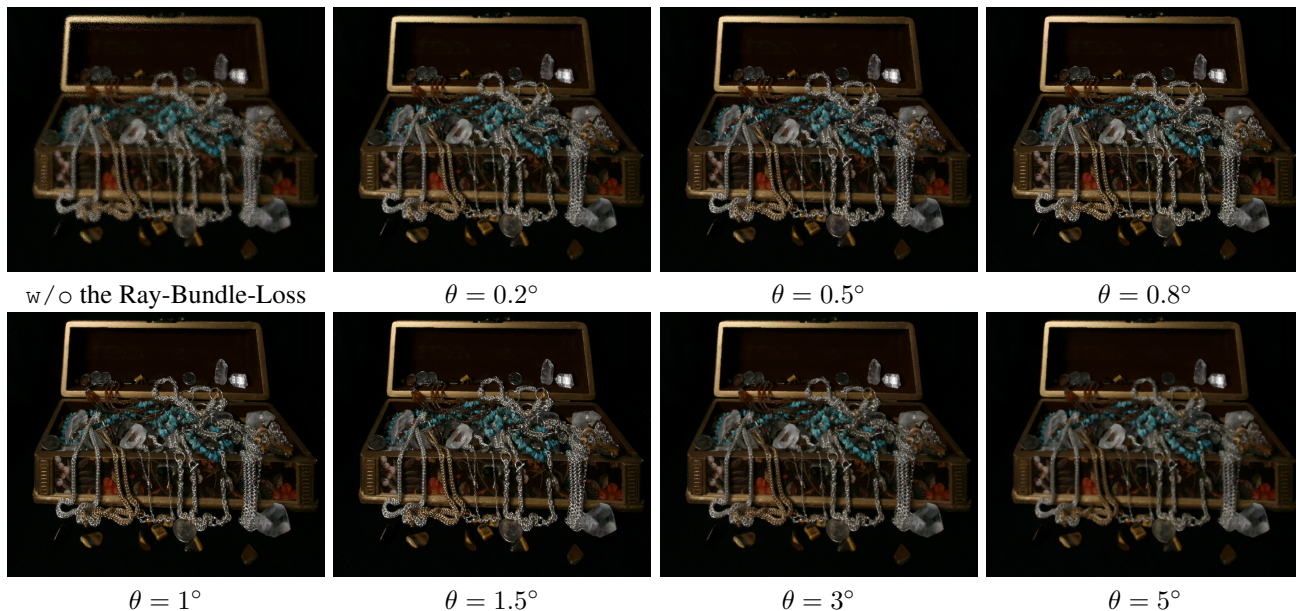


Figure 9: Novel view synthesis results using none and various values of θ . $\theta = 1.5^\circ$ produces the best result for this dataset.

quality between NeRF and NeLF, in Figure 8, we visualize the difference between the ground-truth views and the views rendered by NeRF and NeLF. It shows that both NeRF and NeLF have close to zero difference in the low-frequency area. In the high-frequency area, NeLF has a smaller reconstruction error compared with NeRF.

4.3 Ablation Studies

We use two scenes, the *Treasure Chest* and the *Lego Bulldozer*, which contain complex local details, for ablation studies.

θ in Ray Bundle Loss: In Figure 9, we demonstrate the effectiveness of the Ray Bundle Loss. By training NeLF with a different ray bundle angle θ , we show the resulting synthesized novel views. When θ is too small, the image has aliasing artifacts. On the other hand, when θ is too large, the image will be over-smoothed. $\theta = 1.5$ produces the

best result for this scene. The investigation confirms our hypothesis that an appropriately selected θ according to the imaging parameter is important for producing good results.

Fourier Sparsity and Ray Bundle Loss: In Figure 10, we demonstrate how the Fourier Sparsity Loss \mathcal{L}_s and the Ray Bundle Loss \mathcal{L}_r affect the quality of synthesized views. We display the results of two different scenes, each in a row. We compare the model trained without \mathcal{L}_s (w/o FSL), the model trained without \mathcal{L}_r (w/o RBL), and the model trained with both \mathcal{L}_s and \mathcal{L}_r . The Fourier Sparsity Loss enables novel view synthesis and Ray Bundle Loss further improves the image quality. With both \mathcal{L}_s and \mathcal{L}_r , the model achieves the best quality. In Table 4, we report the scores on each of the models. The scores are computed by averaging the scores on all the scenes in the dataset.

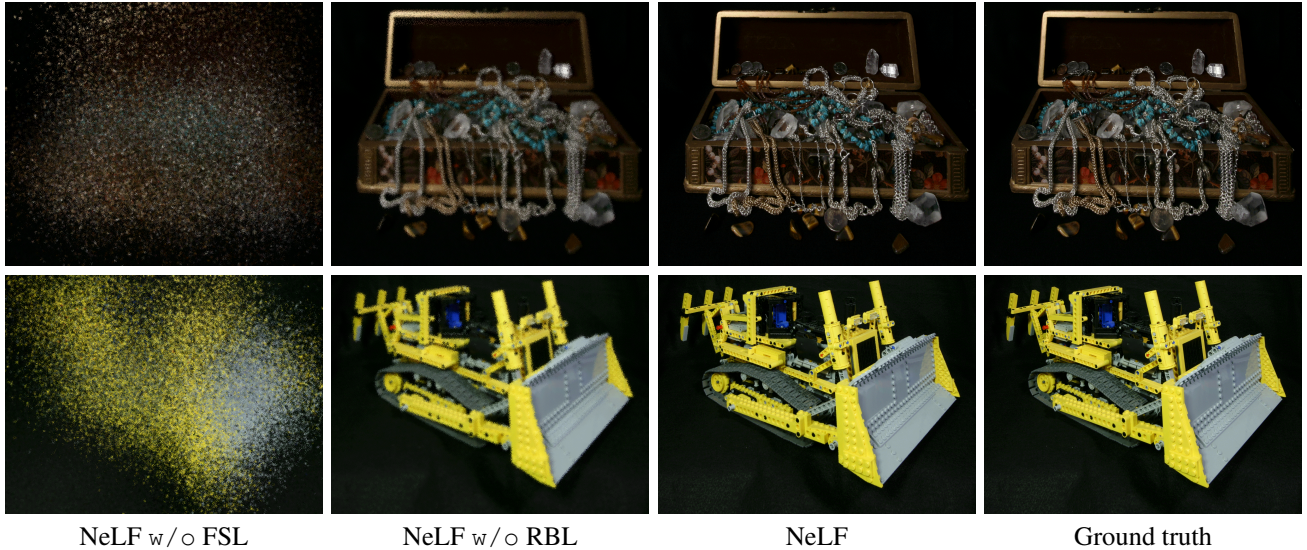


Figure 10: We show results of NeLF trained without \mathcal{L}_s (w/o FSL), without \mathcal{L}_r (w/o RBL), and with both \mathcal{L}_s and \mathcal{L}_r . The last column shows ground truth. The two rows are from two different scenes.

Table 4: A quantitative comparison of NeLF w/o Fourier Sparsity Loss (w/o FSL), NeLF w/o Ray Bundle Loss (w/o RBL) dataset, and NeLF. The scores are computed by averaging the scores on all the scenes in the Stanford Light Field dataset.

	PSNR \uparrow	SSIM \uparrow
NeLF w/o FSL	30.217	0.163
NeLF w/o RBL	32.774	0.591
NeLF	38.180	0.947

4.4 Applications

Novel view synthesis: A trained NeLF models the comprehensive color distribution of all the rays within the baseline of the training set. Therefore, if we restrict the camera location and orientation within small deviations from the capturing camera plane and view direction, we can render a novel view from NeLF by using Eqn. 4. In Figure 11, we show two novel views rendered by a NeLF trained on the *Lego Truck* scene in the dataset. The cameras for these two views are not on the plane of the training camera array, and the viewing direction is not along the z -direction. We can see the view-dependent effects in the zoom-in sub-figures.

Free Viewpoint Video and Non-Planar Camera Configuration: In Figure 13, we demonstrate the result of a NeLF trained on the *Flames* scene in the DeepViewVideo dataset [2]. In this dataset, there are 46 cameras mounted on a semi-sphere surface. We excluded the views which are focusing on the sky or the ground, and selected 27 views as the training data. Although the training views have a non-planar camera configuration, NeLF can still faithfully learn

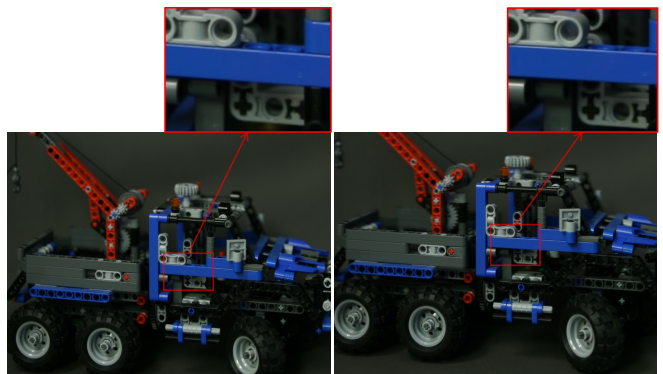


Figure 11: With reconstructed light field, novel view synthesis is supported.

the color distribution of the rays and successfully generate novel views. Moreover, since the dataset contains time-synchronized video, we train NeLFs on the views at different time instances. By rendering the scene with these NeLFs continuously, we can generate free-viewpoint video (FVV) on a dynamic scene. In our demo video, we demonstrate this result.

Refocusing: In Figure 12, we show an example of the refocusing effect on the *Lego Truck* scene in the dataset. Refocusing is enabled naturally by the 4D light field representation.



Figure 12: With reconstructed light field, refocusing is supported.

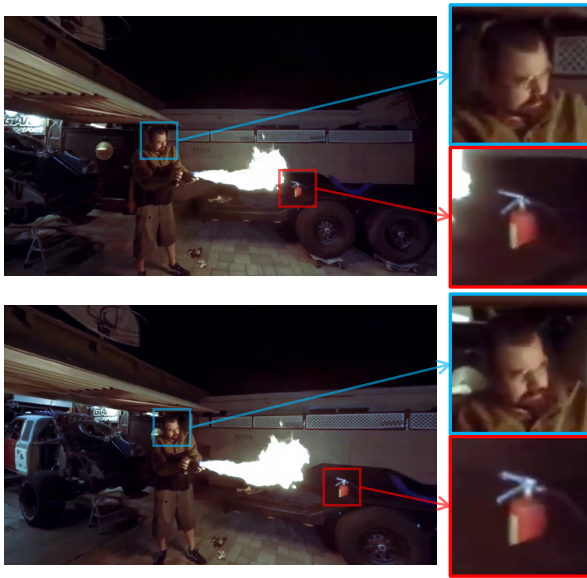


Figure 13: Non-planar camera configuration.

5 Conclusion

We propose a novel view synthesis framework called Neural 4D Light Field (NeLF). Unlike NeRF, we represent a continuous scene using a 4D light field and train an MLP network to learn this mapping from input posed images. By limiting novel view synthesis to include only front views, NeLF can achieve a comparable quality level as NeRF, but achieves a 1000x speedup. Moreover, because the speedup is enabled by modeling the color of light rays, NeLF does not need additional storage for acceleration. To effectively train NeLF, we propose two novel loss terms: Fourier Sparsity Loss and Ray Bundle Loss. We demonstrate state-of-the-art novel view synthesis results, and we also provide ablation studies to show the effectiveness of the loss terms.

6 Limitations and Future Work

There are several limitations to our approach. First, the novel viewpoints are limited to be on the one side of the two light slabs. In the future, we would like to extend the method to use more flexible 4D parameterizations such as multiple two planes, two cylindrical surfaces, or two spherical surfaces. By assuming the color is constant along a ray in free space, NeLF cannot model rays that are blocked by the scene itself; therefore, novel viewpoints are always outside of the convex hull of the scene. This is an inherited limitation from light field.

Instead of using a 4D parameterization, lower-dimensional parameterization for specific applications can also be used. For example, in the work of concentric mosaic [29], by constraining camera motion to planar concentric circles, all input image rays are indexed in three parameters. By adopting this parameterization, a more compact representation of the scene can be achieved, which potentially runs even faster than a 4D parameterization.

Although our simplified NeLF model can significantly improve the rendering speed compared with NeRF, it also has the limitations when it comes to 3D scene structure recovery. In the future, we would like to extend our work to reconstruct the surface from the reconstructed light field by using existing approaches such as Shape from Light Field (SfLF) techniques [8].

References

- [1] J. T. Barron, B. Mildenhall, M. Tancik, P. Hedman, R. Martin-Brualla, and P. P. Srinivasan. Mip-nerf: A multiscale representation for anti-aliasing neural radiance fields. *arXiv preprint arXiv:2103.13415*, 2021.
- [2] M. Broxton, J. Flynn, R. Overbeck, D. Erickson, P. Hedman, M. Duvall, J. Dourgarian, J. Busch, M. Whalen, and P. Debevec. Immersive light field video with a layered mesh representation. *ACM Transactions on Graphics (TOG)*, 39(4):86–1, 2020.

- [3] C. Buehler, M. Bosse, L. McMillan, S. Gortler, and M. Cohen. Unstructured lumigraph rendering. In Proceedings of the 28th Annual Conference on Computer Graphics and Interactive Techniques, SIGGRAPH '01, page 425–432, New York, NY, USA, 2001. Association for Computing Machinery.
- [4] B. Chen, L. Ruan, and M.-L. Lam. Lfgan: 4d light field synthesis from a single rgb image. ACM Transactions on Multimedia Computing, Communications, and Applications (TOMM), 16(1):1–20, 2020.
- [5] J. Flynn, M. Broxton, P. Debevec, M. DuVall, G. Fyffe, R. S. Overbeck, N. Snavely, and R. Tucker. Deepview: High-quality view synthesis by learned gradient descent. In Conference on Computer Vision and Pattern Recognition (CVPR), 2019.
- [6] S. J. Garbin, M. Kowalski, M. Johnson, J. Shotton, and J. Valentin. Fastnerf: High-fidelity neural rendering at 200fps. arXiv preprint arXiv:2103.10380, 2021.
- [7] S. J. Gortler, R. Grzeszczuk, R. Szeliski, and M. F. Cohen. The lumigraph. In Proceedings of the 23rd Annual Conference on Computer Graphics and Interactive Techniques, SIGGRAPH '96, page 43–54, New York, NY, USA, 1996. Association for Computing Machinery.
- [8] S. Heber, W. Yu, and T. Pock. Neural epi-volume networks for shape from light field. In Proceedings of the IEEE International Conference on Computer Vision, pages 2252–2260, 2017.
- [9] P. Hedman, J. Philip, T. Price, J.-M. Frahm, G. Drettakis, and G. Brostow. Deep blending for free-viewpoint image-based rendering. 37(6):257:1–257:15, 2018.
- [10] A. Isaksen, L. McMillan, and S. J. Gortler. Dynamically reparameterized light fields. In Proceedings of the 27th Annual Conference on Computer Graphics and Interactive Techniques, SIGGRAPH '00, page 297–306, USA, 2000. ACM Press/Addison-Wesley Publishing Co.
- [11] A. Kanazawa, S. Tulsiani, A. A. Efros, and J. Malik. Learning category-specific mesh reconstruction from image collections. In Proceedings of the European Conference on Computer Vision (ECCV), pages 371–386, 2018.
- [12] P. Kellnhofer, L. Jebe, A. Jones, R. Spicer, K. Pulli, and G. Wetzstein. Neural lumigraph rendering. arXiv preprint arXiv:2103.11571, 2021.
- [13] D. P. Kingma and J. Ba. Adam: A method for stochastic optimization. arXiv preprint arXiv:1412.6980, 2014.
- [14] M. Levoy and P. Hanrahan. Light field rendering. In Proceedings of the 23rd annual conference on Computer graphics and interactive techniques, pages 31–42, 1996.
- [15] D. Lindell, J. Martel, and G. Wetzstein. AutoInt: Automatic integration for fast neural volume rendering. <https://arxiv.org/abs/2012.01714>, 2020.
- [16] L. Liu, J. Gu, K. Z. Lin, T.-S. Chua, and C. Theobalt. Neural sparse voxel fields. In Advances in Neural Information Processing Systems (NeurIPS), volume 33, 2020.
- [17] S. Lombardi, T. Simon, J. Saragih, G. Schwartz, A. Lehrmann, and Y. Sheikh. Neural volumes: Learning dynamic renderable volumes from images. ACM Trans. Graph., 2019.
- [18] S. Lombardi, T. Simon, G. Schwartz, M. Zollhoefer, Y. Sheikh, and J. Saragih. Mixture of volumetric primitives for efficient neural rendering, 2021.
- [19] R. Martin-Brualla, N. Radwan, M. Sajjadi, J. T. Barron, A. Dosovitskiy, and D. Duckworth. NeRF in the wild: Neural radiance fields for unconstrained photo collections. <https://arxiv.org/abs/2008.02268>, 2020.
- [20] N. Meng, X. Wu, J. Liu, and E. Lam. High-order residual network for light field super-resolution. In Proceedings of the AAAI Conference on Artificial Intelligence, volume 34, pages 11757–11764, 2020.
- [21] B. Mildenhall, P. P. Srinivasan, R. Ortiz-Cayon, N. K. Kalantari, R. Ramamoorthi, R. Ng, and A. Kar. Local light field fusion: Practical view synthesis with prescriptive sampling guidelines. ACM Transactions on Graphics (TOG), 38(4):1–14, 2019.
- [22] B. Mildenhall, P. P. Srinivasan, M. Tancik, J. T. Barron, R. Ramamoorthi, and R. Ng. Nerf: Representing scenes as neural radiance fields for view synthesis. In European Conference on Computer Vision, pages 405–421. Springer, 2020.
- [23] T. Neff, P. Stadlbauer, M. Parger, A. Kurz, C. R. A. Chaitanya, A. Kaplanyan, and M. Steinberger. Donerf: Towards real-time rendering of neural radiance fields using depth oracle networks. arXiv preprint arXiv:2103.03231, 2021.

- [24] K. Park, U. Sinha, J. T. Barron, S. Bouaziz, D. Goldman, S. Seitz, and R. Martin-Brualla. Deformable neural radiance fields. <https://arxiv.org/abs/2011.12948>, 2020.
- [25] C. Reiser, S. Peng, Y. Liao, and A. Geiger. Kilonerf: Speeding up neural radiance fields with thousands of tiny mlps, 2021.
- [26] G. Riegler and V. Koltun. Free view synthesis. In *European Conference on Computer Vision*, 2020.
- [27] S. Saito, Z. Huang, R. Natsume, S. Morishima, H. Li, and A. Kanazawa. Pifu: Pixel-aligned implicit function for high-resolution clothed human digitization. In *2019 IEEE/CVF International Conference on Computer Vision (ICCV)*, pages 2304–2314, 2019.
- [28] L. Shi, H. Hassanieh, A. Davis, D. Katabi, and F. Durand. Light field reconstruction using sparsity in the continuous fourier domain. *ACM Transactions on Graphics (TOG)*, 34(1):1–13, 2014.
- [29] H.-Y. Shum and L.-W. He. Rendering with concentric mosaics. In *Proceedings of the 26th annual conference on Computer graphics and interactive techniques*, pages 299–306, 1999.
- [30] V. Sitzmann, J. Martel, A. Bergman, D. Lindell, and G. Wetzstein. Implicit neural representations with periodic activation functions. *Advances in Neural Information Processing Systems*, 33, 2020.
- [31] V. Sitzmann, J. Thies, F. Heide, M. Nießner, G. Wetzstein, and M. Zollhöfer. Deepvoxels: Learning persistent 3d feature embeddings. In *Proc. Computer Vision and Pattern Recognition (CVPR)*, IEEE, 2019.
- [32] V. Sitzmann, M. Zollhoefer, and G. Wetzstein. Scene representation networks: Continuous 3d-structure-aware neural scene representations. In *Advances in Neural Information Processing Systems*, volume 32, 2019.
- [33] P. P. Srinivasan, B. Deng, X. Zhang, M. Tancik, B. Mildenhall, and J. T. Barron. Nerv: Neural reflectance and visibility fields for relighting and view synthesis. *arXiv preprint arXiv:2012.03927*, 2020.
- [34] P. P. Srinivasan, R. Tucker, J. T. Barron, R. Ramamoorthi, R. Ng, and N. Snavely. Pushing the boundaries of view extrapolation with multiplane images. In *Proceedings of the IEEE/CVF Conference on Computer Vision and Pattern Recognition*, pages 175–184, 2019.
- [35] M. Tancik, P. P. Srinivasan, B. Mildenhall, S. Fridovich-Keil, N. Raghavan, U. Singhal, R. Ramamoorthi, J. T. Barron, and R. Ng. Fourier features let networks learn high frequency functions in low dimensional domains. *arXiv preprint arXiv:2006.10739*, 2020.
- [36] A. Tewari, O. Fried, J. Thies, V. Sitzmann, S. Lombardi, K. Sunkavalli, R. Martin-Brualla, T. Simon, J. Saragih, M. Nießner, R. Pandey, S. Fanello, G. Wetzstein, J.-Y. Zhu, C. Theobalt, M. Agrawala, E. Shechtman, D. B. Goldman, and M. Zollhöfer. State of the Art on Neural Rendering. *Computer Graphics Forum (EG STAR 2020)*, 2020.
- [37] Z. Wang, S. Wu, W. Xie, M. Chen, and V. A. Prisacariu. Nerf —: Neural radiance fields without known camera parameters. *arXiv preprint arXiv:2102.07064*, 2021.
- [38] B. Wilburn, N. Joshi, V. Vaish, E.-V. Talvala, E. Antunez, A. Barth, A. Adams, M. Horowitz, and M. Levoy. High performance imaging using large camera arrays. In *ACM SIGGRAPH 2005 Papers*, pages 765–776. 2005.
- [39] S. Wizadwongsa, P. Phongthawee, J. Yenphraphai, and S. Suwajanakorn. Nex: Real-time view synthesis with neural basis expansion. In *Conference on Computer Vision and Pattern Recognition (CVPR)*, 2021.
- [40] G. Wu, Y. Liu, L. Fang, and T. Chai. Revisiting light field rendering with deep anti-aliasing neural network. *IEEE Transactions on Pattern Analysis and Machine Intelligence*, 2021.
- [41] L. Yariv, Y. Kasten, D. Moran, M. Galun, M. Atzmon, B. Ronen, and Y. Lipman. Multiview neural surface reconstruction by disentangling geometry and appearance. *Advances in Neural Information Processing Systems*, 33, 2020.
- [42] A. Yu, R. Li, M. Tancik, H. Li, R. Ng, and A. Kanazawa. Plenotrees for real-time rendering of neural radiance fields. *arXiv preprint arXiv:2103.14024*, 2021.
- [43] K. Zhang, G. Riegler, N. Snavely, and V. Koltun. Nerf++: Analyzing and improving neural radiance fields. *arXiv preprint arXiv:2010.07492*, 2020.
- [44] X. Zhang, S. Fanello, Y.-T. Tsai, T. Sun, T. Xue, R. Pandey, S. Orts-Escolano, P. Davidson, C. Rheemann, P. Debevec, et al. Neural light transport for relighting and view synthesis. *ACM Transactions on Graphics (TOG)*, 40(1):1–17, 2021.

- [45] T. Zhou, R. Tucker, J. Flynn, G. Fyffe, and N. Snavely. Stereo magnification: Learning view synthesis using multiplane images. *ACM Trans. Graph.*, 37(4), July 2018.